Nozzle-Quenching Process for Controlled Flame Synthesis of Titania Nanoparticles

Karsten Wegner and Sotiris E. Pratsinis
Particle Technology Laboratory, Dept. of Mechanical and Process Engineering, ML F25, ETH Zürich, CH-8092 Zürich, Switzerland

A process for precisely controlled synthesis of nanoparticles with a broad range of sizes, morphologies, and phase compositions is presented. This is achieved by a rapid quenching of the entire flame aerosol in a critical-flow nozzle placed above and into the flame. This process is evaluated for synthesis of titania nanoparticles by oxidation of titanium-tetra-isopropoxide (TTIP) in a methane/oxygen coflow diffusion-flame reactor. Precise control of phase composition from 97 to 5 wt. % anatase (and the balance rutile) and average primary particle diameter from 5 to 60 nm is possible by positioning the quenching nozzle at the desired heights above the burner and controlling gas and precursor flow rates. The nozzle quenching also reduces the degree of agglomeration of the product particles. An operation diagram shows that the primary particle diameter and the phase composition can be independently controlled, making anatase or rutile nanoparticles with high or low specific surface area.

Introduction

Combustion synthesis has been used to produce a wide range of oxide nanoparticles (Ulrich, 1984), nonoxide ceramics (Dufaux and Axelbaum 1995; Glassman et al., 1992), and even pure metals (Calcote and Felder, 1992). Among these processes, flame aerosol synthesis of carbon black, titania, and silica are the most important ones industrially, as is apparent from an annual production volume of several million metric tons and particle production rates up to 25 metric tons per hour.

Coflow diffusion flame aerosol reactors, in particular, offer high flexibility by broad operation windows and safety (no flash back). Temperature fields and particle residence times in these reactors, both key parameters for particle growth (Formenti et al., 1972), can be controlled by changing the reactant mixing configuration or varying the reactant flow rates (Pratsinis et al., 1996). However, the range of accessible product powders is still restricted, since the flame temperature and the length of the particle growth zone determining the particle residence time are coupled. Typically, flame-made oxide particles grow by coagulation–coalescence from perfectly spherical particles to agglomerated ones, as has been shown by thermophoretic sampling and transmission electron microscopy (Arabi-Katbi et al., 2001). The high flame temperatures necessary for complete coalescence of the refractory compounds usually go along with extended particle growth zones, while short flames exhibit lower temperatures, as was shown by computational fluid dynamics for coflow diffusion flames making titania (Johannessen et al., 2001). As a result, spherical particles with a low degree of agglomeration made in hot flames usually have primary particle diameters of 100 nm and above, while colder flames typically produce highly agglomerated primary particles with diameters down to a few nanometers (Zhu and Pratsinis, 1996). Control of agglomeration has been achieved with sodium flames (Dufaux and Axelbaum, 1995), and low-pressure flames (Glumac et al., 1998), but is still limited in classic flame aerosol reactors, making it difficult to attain nonagglomerate particles smaller than about 100 nm with these units (Pratsinis, 1998). Such nonagglomerated nanoparticles are, however, of key interest as starting material for ceramics as dense particle packing can be achieved (Barringer et al., 1984; Calcote et al., 1990).

Here, a flame aerosol process is presented allowing precise control of the flame length and product particle size independently of the reactant flow rates. This is achieved by quenching the entire flame in a critical flow nozzle, which rapidly

Correspondence concerning this article should be addressed to S. E. Pratsinis.

stops particle growth (Wegner et al., 2002). The aerosol quenching effect relies on gas expansion and mixing with ambient air drawn into the nozzle. Quenching techniques by jet expansion have been applied to combustion synthesis for sampling from the product flow stream of flame aerosol reactors (Ulrich et al., 1976; Lindackers et al., 1997) or product separation and collection (Calcote and Felder, 1992). Also, quenching by cross flow air has been used in flame synthesis of titania and silica (Rulison et al., 1996) as well as zinc oxide nanoparticles (Hansen et al., 2001). Here, critical nozzle flow quenching is systematically investigated as it is directly applied on an atmospheric pressure coflow diffusion flame producing titania nanoparticles that are characterized by transmission electron microscopy, X-ray diffraction, and nitrogen adsorption. The effect of the burner–nozzle distance on product particle characteristics is investigated at various precursor and oxidant flow rates, and an operation diagram relating BET–equivalent diameter and phase composition of the product titania particles is developed.

Experimental Studies

Figure 1 shows the experimental setup. A coflow diffusion flame aerosol reactor consisting of three concentric stainless-steel tubes was used. The inner diameters of the tubes were 1.8, 3.5, and 4.8 mm, and the tube wall thickness was 0.3 mm. An argon stream of 0.75 L/min carrying TTIP (Aldrich, purity > 97%) vapor from an evaporator (Bronkhorst CEM, 100 W) was introduced through the center tube, 0.5 L/min methane flowed through the first annulus, and 2–6 L/min oxygen was provided through the outer annulus. The flow rates of all gases (Pan Gas, purity > 99.999%) were monitored by calibrated mass-flow controllers. The TTIP liquid flow rate into the evaporator was controlled by a liquid mass-flow meter (Bronkhorst Liqui-Flow). The evaporator, precursor delivery tubes, and burner were heated to 150°C to prevent TTIP condensation.

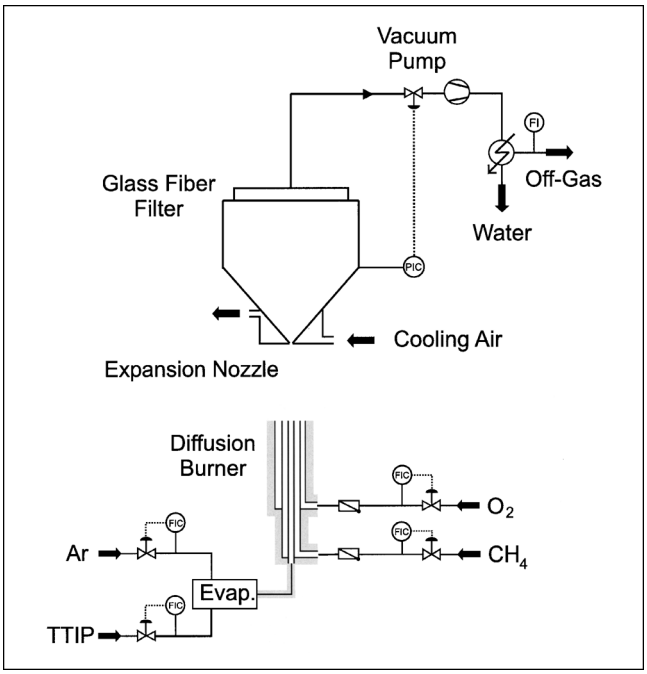

Figure 1. Experimental setup with the reactant delivery system, diffusion flame reactor, quenching nozzle, and glass-fiber filter.

A critical-flow nozzle connected with a cylinder (ID = 140 mm) to a filter holder with a glass-fiber filter (Whatman GF/A) formed a gas expansion–particle collection unit that was positioned 0.5–8 cm above the burner mouth. The air-cooled stainless-steel expansion nozzle had a flat bottom at the side facing the burner with a 1.5-mm nozzle bore at the center that opened conically toward the filter. A 3-stage positioning system (Föhrenbach Unipos) was used to align the burner center axis with the nozzle bore (accuracy $\pm$0.5 mm) and to select the distance between burner and nozzle. Throughout the experiments, a pressure of 150 mbar was maintained in the expansion chamber by a butterfly valve in the off-gas line. Product titania particles were collected on the filter with the aid of a vacuum pump. A rotameter connected behind a condenser at the outlet of the vacuum pump allowed the determination of the gas flow rate through the nozzle. A change in the expansion chamber pressure to 100 and 200 mbar did not result in a change in the flow rate through the nozzle, showing that sonic flow conditions were prevalent in the nozzle (Perry and Green, 1984). Particles were produced at 2 to 6 L/min oxygen flow rate, 6.5 g/h TTIP flow rate, and burner-nozzle distances (BND) of 0.5–8 cm, as well as by varying the TTIP flow rate from 1.63 g/h to 26 g/h at constant carrier-gas flow rate.

Center-line temperature measurements in the flame were made with a 0.5-mm thin wire Pt-Rh thermocouple (Type B, Omega Engineering) in the absence of TTIP. The TTIP concentrations used would have raised the temperature by approximately 100–200°C (Arabi-Katbi et al., 2001). The spatial resolution of the flame temperature measurement was 0.2 cm, and the obtained data were corrected for heat loss by radiation, using an emissivity of 0.18 for the Pt wire. The center-line temperature downstream of the nozzle was recorded with a 1-mm R-type thermocouple at a distance of 0.8 cm from the nozzle exit.

The specific surface area (SSA) of the collected powders was analyzed by nitrogen adsorption at 77 K, using the BET isotherm (Micromeritics TriStar 3000). Assuming all particles to be monodisperse spheres, the BET–equivalent particle diameter was calculated as $d_p = 6 / (\rho_{TiO_2} \times SSA)$, where ρ_{TiO_2} is the weighted density of the particles ($\rho_{Rutile} = 4.26$ g/cm^3 and $\rho_{Anatase} = 3.84$ g/cm^3). X-Ray diffraction (XRD) patterns of all powders were obtained with a Bruker D8 advance diffractometer operating with Cu(K_α) radiation. Crystallite size and phase composition were obtained using the Rietveld method and the fundamental parameter approach (Cheary and Coelho, 1992). Particle samples for analysis by transmission electron microscopy (TEM, Hitachi H600, 100 kV) were collected by thermophoresis (Dobbins and Megaridis, 1987) at various heights in the flame and at 8 cm downstream of the nozzle. In experiments without the nozzle, product particles were sampled at the center line in front of the filter, about 15 cm downstream of the visible flame. High-resolution TEM investigations (HRTEM, Philips CM30ST, 300 kV) were performed on product particles deposited onto carbon-coated copper grids.

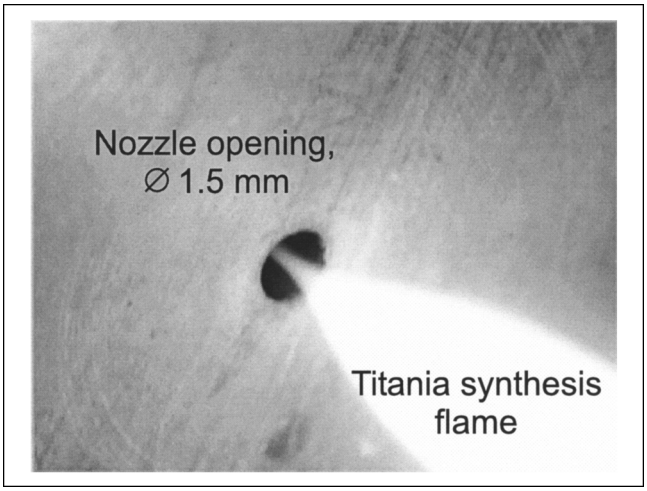

Figure 2. Titania particle-laden flame contracted into the nozzle, enveloped by a sheath of ambient air.

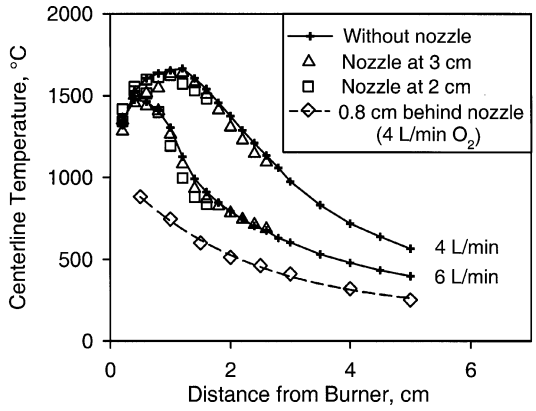

Figure 3. Center-line temperatures of flames with 4 and 6 L/min oxygen flow rate without the nozzle (crosses) and with the quenching nozzle placed 2 (squares) and 3 cm (triangles) above the burner.

Center-line temperatures measured 0.8 cm downstream from the nozzle at 4 L/min O_2 flow rate (diamonds) for burner–nozzle distances of 0.5 to 5 cm show that nozzle quenching decreases the downstream gas temperature by 250–770°C.

Results and Discussion

Flame characterization

Figure 2 shows how a particle-laden flame (6.5 g/h TTIP in 0.75 L/min Ar, 0.5 L/min CH_4, and 2 L/min O_2) is drawn into the nozzle. At a short distance in front of the nozzle bore, the flame is contracted and confined to the region close to the center axis. In addition to the flame aerosol, ambient air is drawn into the nozzle, forming an enveloping sheath around the particle-laden combustion gases, thus preventing clogging of the nozzle and particle deposition. Determination of the off-gas flow rate at the outlet of the vacuum pump showed that, depending on burner-nozzle distance and flame temperature, 7–9 L/min of ambient air are drawn into the nozzle for the flame with a 2-L/min O_2 flow rate. The sheath air rapidly mixes, quenches, and dilutes the hot flame aerosol by 2–3 times in the expansion chamber downstream of the nozzle.

Figure 3 shows the center-line temperatures of the coflow methane diffusion flame with 4 and 6 L/min oxygen flow without (crossed lines) and with the nozzle at 2 cm (squares) and 3 cm (triangles) above the burner. With 4-L/min oxygen flow and without the nozzle, the maximum flame temperature is about 1,650°C at 1.2 cm above the burner, and drops to 550°C at 5 cm above the burner. This temperature decrease is attributed to mixing of the combustion gases with excess supplied oxygen and entrainment of ambient air (Wegner and Pratsinis, 2002). When the nozzle is placed at 2 or 3 cm above the burner (Figure 3), the center-line temperature up to 0.6 cm in front of the nozzle drops by less than 100°C compared to that obtained without the nozzle. This indicates that the entrained air from the nozzle does not significantly influence the flame upstream of the nozzle. Temperature measurements closer to the nozzle were not made, since the thermocouple notably disturbed the contracted flame directly in front of the nozzle. Figure 2 indicates, however, that at short distances (<1 cm) in front of the nozzle the flame is influenced by the ambient quenching air drawn into the nozzle. For the flame with a 6-L/min oxygen flow rate the maximum temperature is 1,500°C at 0.4 cm above the burner and drops to 400°C at 5 cm. In general, increasing O_2 flow rates result in a steeper temperature drop downstream of the burner due to rapid mixing with excess supplied oxygen. When the nozzle is placed at 2 and 3 cm in the 6-L/min O_2 flame, the upstream center-line temperature is not influenced, supporting the results for the flame with a 4-L/min O_2 flow rate.

Figure 3 also shows the center-line temperature 0.8 cm downstream from the nozzle opening (diamonds) for burner–nozzle distances (BND) of 0.5 to 5 cm and the 4-L/min oxygen flame. The highest temperature of 880°C was measured for 0.5 cm BND, the lowest (250°C) for 5-cm BND. Thus, the nozzle decreases the temperature by 770°C and 250°C at 1.3 cm (0.5-cm BND) and 4.8 cm (4-cm BND) above the burner, respectively. Downstream nozzle temperatures for the 2 L/min O_2 flame were up to 100°C higher while those for the flame with 6-L/min O_2 flow rate were up to 50°C lower.

Particle size and morphology

Figure 4 depicts the BET–equivalent diameter (circles, left axis) and phase composition (squares, right axis) of titania particles produced without the quenching nozzle as a function of the oxygen flow rate along with typical TEM pictures of product powders made at 2- and 6-L/min oxygen flow. Increasing the oxygen flow rate from 2 L/min to 6 L/min decreased the BET–equivalent particle diameter from 60 nm to 18 nm, in agreement with Zhu and Pratsinis (1996) for titania from $TiCl_4$ in similar methane/oxygen coflow diffusion flames. This is attributed to shorter particle residence times at high temperatures with an increasing oxygen flow rate (Figure 3). Surplus oxygen that is not taking part in combustion and increased entrainment of ambient air from higher oxygen outlet velocity (Johannessen et al., 2001) shorten and cool the flame, resulting in slower sintering and smaller primary particle diameters.

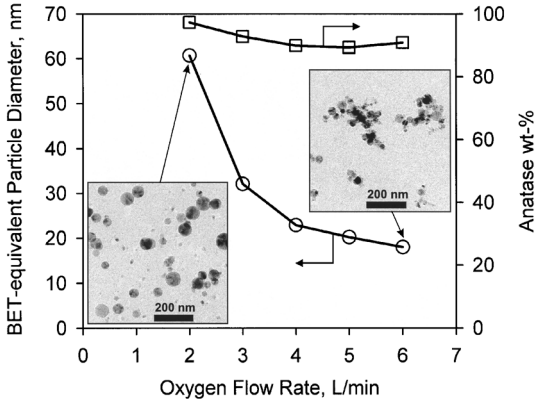

Figure 4. BET-equivalent diameter (circles, left axis) and anatase weight fraction (squares, right axis) of product titania particles as a function of the oxygen flow rate into the diffusion burner made without the quenching nozzle.

Increasing the oxygen flow decreases the primary particle size and decreases the anatase content, but increases the degree of agglomeration (TEM pictures for 2 and 6 L/min O_2 flow rate).

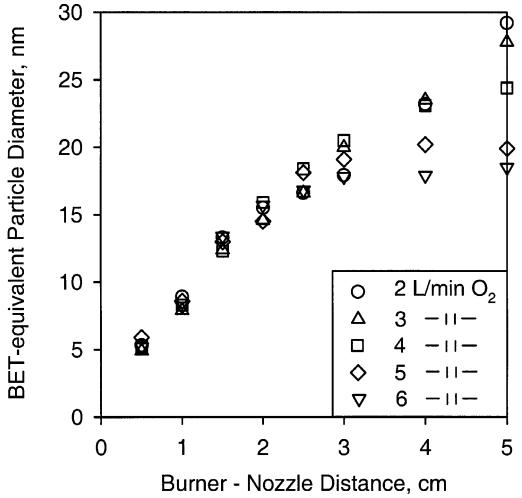

Figure 5. BET-equivalent diameter of titania particles made with the quenching nozzle and oxygen flow rates of 2 to 6 L/min as a function of the burner–nozzle distance. Flame aerosol quenching early in the flame decreases the average primary-particle diameter.

Figure 4 shows that all powders were ≥ 90 wt. % anatase, independent of the oxygen flow rate, in agreement with Zhu and Pratsinis (1996) for methane–oxygen diffusion flames and $TiCl_4$ oxidation in excess O_2. The TEM pictures in Figure 4 show that titania product particles made in the flame with 2-L/min oxygen flow were spheres with little agglomeration, indicating long particle residence times at high temperatures. In contrast, the shorter flame with 6-L/min oxygen flow rate produced agglomerate particles, consistent with Pratsinis et al. (1996) and Johannessen et al. (2001).

Figure 5 shows the BET–equivalent diameter of titania nanoparticles made with the quenching nozzle in flames with oxygen flow rates of 2–6 L/min as a function of the BND. At BND = 0.5 cm, product particles of 5 nm BET–equivalent diameter were obtained, regardless of the oxygen flow rate. These primary particles were 3–10 times smaller than those made without the nozzle (Figure 4), showing that nozzle quenching effectively freezes particle growth. The independence of the average primary particle diameter from the oxygen flow rate for BNDs up to 2 cm indicates that nozzle quenching had arrested particle growth before excess oxygen flow had a chance to affect the late particle growth process. This may indicate further that flame temperatures were high enough for these particle sizes to allow rapid coalescence after particle collisions (Wu et al., 1993). By observing titania sintering in a hot-stage electron microscope, George et al. (1973) reported a critical sintering temperature of 840°C for rapid coalescence of titania nanoparticles similarly sized with the ones studied here. The center-line temperature profiles of the particle-free flames (Figure 3) show that even the shortest flame (6-L/min oxygen flow rate) exhibited temperatures above 800°C in this region. Temperatures in the particle-laden flame are expected to be even higher, since the combustion of TTIP is an exothermic reaction (combustion enthalpy: −8088 kJ/mol, Bradley et al., 1978), accounting for about 15 % of the total combustion enthalpy for the present flames. This supports the assumption that titania particle growth in the high temperature region (up to 2 cm above the burner) is governed by coagulation, as coalescence is rapid and independent of the flame temperature for these particle sizes (Figure 5).

At BNDs above 3 cm, product nanoparticles made with 6-L/min O_2 flow had approached the size of 18 nm, which is identical to that obtained without the quenching nozzle (Figure 4). At these distances, the nozzle was located well above the visible flame height and temperatures were less than 600°C (Figure 3). At these low temperatures, primary particle growth by sintering was already rather slow and the additional cooling coming from the nozzle quenching did not affect the product particle size. For oxygen flow rates of 5 and 4 L/min, this limit was reached at BNDs of 4 and 5 cm, respectively, where the same product primary particle size of 20 nm (5 L/min O_2) and 23 nm (4 L/min O_2) was obtained with and without the nozzle. At BND = 4 cm, the temperature of the flame with 4-L/min oxygen flow rate had fallen just below the characteristic temperature for rapid coalescence of these particle sizes (Figure 3), which is consistent with the data of the 6-L/min O_2 flame. In flames with 3- and 2-L/min oxygen flow rates, particle growth could still be controlled with the quenching nozzle at 5-cm BND, as these flames have a longer high-temperature zone than the flames using high oxygen flow rates. The BET-equivalent particle diameters were 28 nm and 29 nm, while those obtained without the quenching nozzle (Figure 4) were 32 and 60 nm for the 3- and 2-L/min O_2 flames, respectively. This shows that the operation window of the coflow diffusion flame reactor (Figure 4) could be extended to smaller primary particle sizes by the quenching nozzle controlling the flame length, and, therefore, the particle residence time at high temperature.

Figure 6 shows TEM pictures of titania particles thermophoretically sampled from the center line of the 2-L/min

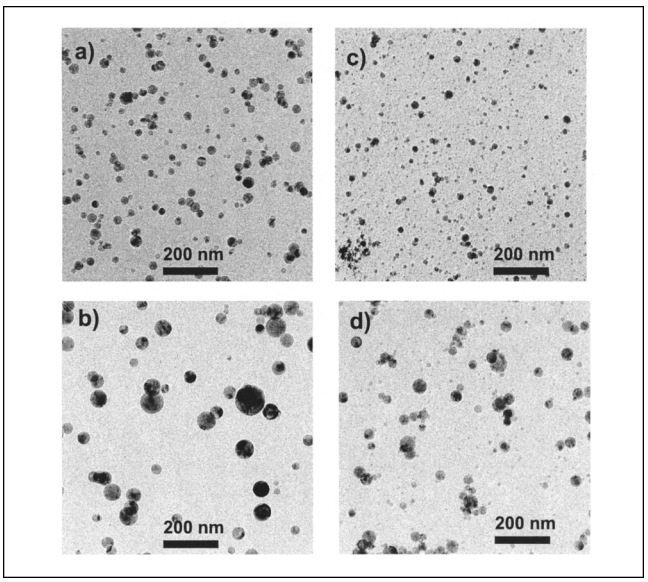

Figure 6. TEM pictures of titania particles sampled from the 2 L/min O_2 flame without nozzle at (a) 1 cm and (b) 5 cm above the burner, and those of particles sampled 8 cm downstream of the nozzle for burner–nozzle distances of (c) 1 cm and (d) 5 cm.

The nonagglomerate state of the flame aerosol is preserved after nozzle quenching.

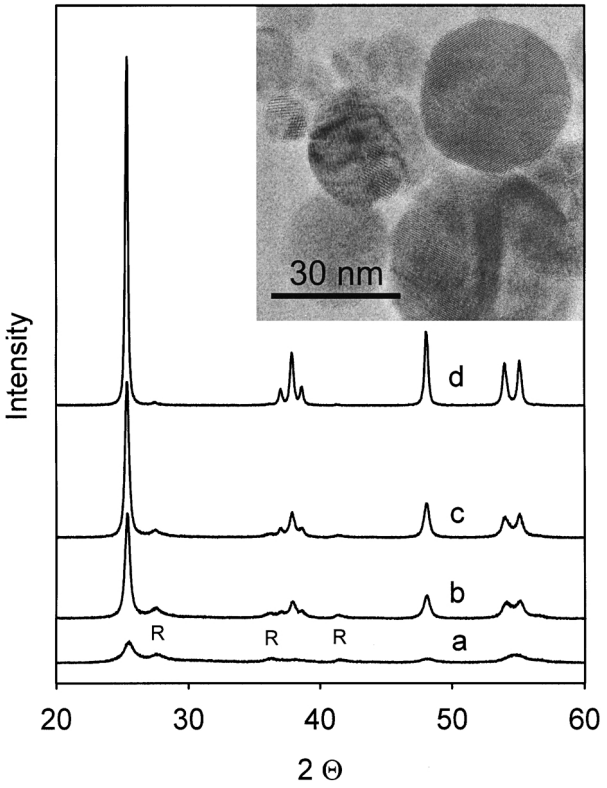

Figure 7. XRD patterns of product powders made in the 2-L/min oxygen flame and 6.5-g/h TTIP flow rate with the quenching nozzle at (a) 1, (b) 3, (c) 5 cm BND, and (d) without the nozzle.

Early quenching in the flame increases the amount of rutile and decreases the average crystallite sizes. The powder made without the nozzle is predominantly anatase titania. The inserted HRTEM picture shows monocrystalline titania nanoparticles made with 5 cm BND.

O_2 flame at (a) 1 cm and (b) 5 cm above the burner in the absence of the nozzle. The titania particles are nonagglomerated spheres growing by rapid coalescence upon collision with increasing distance from the burner. Figure 6 also presents the corresponding TEMs of particles collected at the filter, but with the nozzle at BNDs of 1 cm (Figure 6c) and 5 cm (Figure 6d). These particles are significantly smaller than the ones collected on the filter in the absence of the nozzle (inset of Figure 4) and consistent with the BET data (Figure 5). In addition, these particles have maintained their spherical shape and low degree of agglomeration after nozzle quenching for both BNDs. This indicates that the quenching rates achieved with the nozzle are high enough to suppress further particle growth and possible agglomeration at temperatures where sintering is effective [below about 800°C for the titania particle sizes employed here (George et al., 1973)]. The size of the nozzle-quenched particles (Figures 6c and 6d) is slightly smaller than that observed with particles thermophoretically sampled from the flame at the corresponding distance from the burner (Figure 6a and 6b). This is attributed to the mixing of particles of different flame streamlines in the nozzle. Thus, a sample taken downstream of the nozzle represents the whole flame aerosol population, while the one taken thermophoretically from the flame center line is rather free of particles from the flame boundaries (Arabi-Katbi et al., 2001).

Particle crystallinity

Figure 7 shows X-ray diffraction patterns of powders produced in the flame with 2-L/min O_2 flow rate with the nozzle at BNDs of (a) 1, (b) 3, and (c) 5 cm, and (d) without the nozzle. Without the nozzle, the diffraction pattern of the product powder shows the characteristic reflections of anatase titania and only a small rutile reflection at 27.45° corresponding to the rutile 110 plane (Figure 7d). The phase composition of this powder is 97 wt. % anatase (Figure 4), as determined by the fundamental-parameter approach (Cheary and Coelho, 1992). The diffraction patterns of product powders made with the nozzle show the characteristic reflections of anatase and rutile, with the anatase reflections becoming predominant at larger BND. Decreased peak broadening with increasing BND shows that the crystallites grew larger at longer residence time in the flame, in agreement with the increase in average primary-particle diameter (Figures 5 and 6). An amorphous scattering hump is not observed in any of the diffraction patterns, indicating that all powders were highly crystalline. This is also apparent from the HRTEM micrograph of particles made at 5-cm BND and 2-L/min O_2 flow rate that is inserted in Figure 7. Lattice fringes are discernible to the surface of the particles, indicating that most particles made at this BND are single crystals, in agreement with Stark et al. (2001) for vanadia-coated titania made with this flame reactor.

Figure 8 depicts the phase composition of the powders made with 2- L/min O_2 flow along with that of powders made

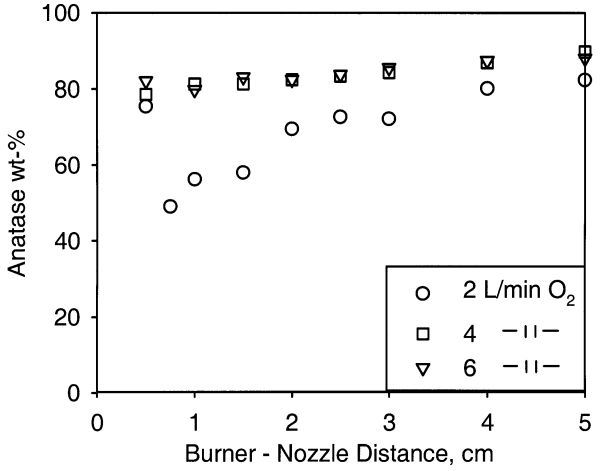

Figure 8. Anatase weight fraction of product powders made without the nozzle and with the nozzle at 0.5 to 5 cm BND in flames with 2- (circles), 4- (squares), and 6-L/min (triangles) oxygen flow rate; anatase is formed in flames with high oxygen flow rates and large BNDs.

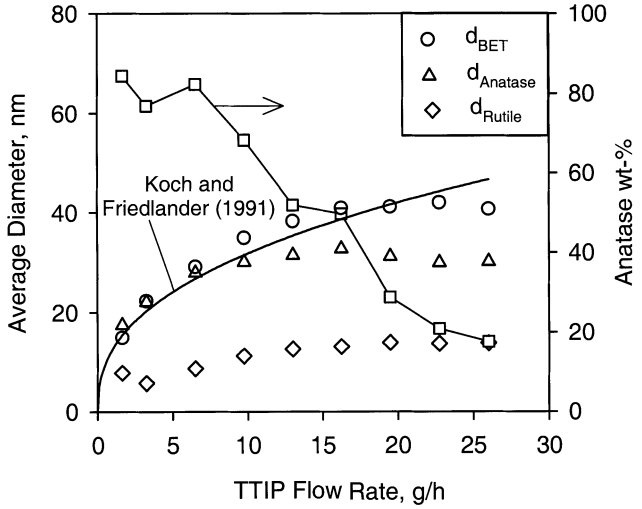

Figure 9. BET-equivalent particle diameter (circles, left axis), anatase (triangles, left axis), and rutile (diamonds, left axis), average crystallite size as well as phase composition (squares, right axis) of product powders made in flames with 2-L/min oxygen flow rate and the quenching nozzle placed at 5 cm above the burner for TTIP flow rates of 1.6 to 26 g/h.

While the anatase weight fraction decreases with increasing TTIP flow rate, the BET-equivalent particle diameter increases following the 2/5 power-law dependence given by Koch and Friedlander (1991) for aerosol coagulation and coalescence in the free molecular regime (solid thick line).

in flames with 4- (squares) and 6-L/min (triangles) oxygen flow rates as a function of the BND. For 2-L/min O_2 flow the anatase weight fraction increases from 56 wt. % to 84 wt. % when the BND is increased from 1 cm to 5 cm. Powders made at 0.5-cm BND, however, had a much higher anatase content of 75 wt. %. At this short BND, the flame structure was significantly affected by flame contraction into the nozzle (Figure 2). Along with the entrainment of sheath air, this increased reactant mixing and accelerated aerosol cooling, resulting in small anatase particles. When reactant mixing was increased by increasing the oxygen flow rate to 4 and 6 L/min, similar phase compositions of 79 (4 L/min) and 82 wt. % (6 L/min) anatase were obtained with 0.5-cm BND. For these turbulent and oxygen-rich flames, the effect of the BND on the product powder phase composition was less significant than for the flame with 2-L/min oxygen flow rate resulting in 90 and 88 wt. % anatase for 4- and 6-L/min O_2 flow rates, respectively, and 5-cm BND. These results indicate that anatase titania is preferentially formed in the flame-nozzle process at high oxygen flow rates. Also, anatase formation is promoted over rutile formation at large BNDs corresponding to long particle residence times and moderate quenching by rather small temperature differences across the nozzle (such as 250°C at 4-cm BND, Figure 3).

Figure 9 shows the influence of the TTIP flow rate (concentration) on the anatase weight fraction (squares), the average crystallite size of anatase (triangles), and rutile (diamonds), as well as the BET−equivalent particle diameter (circles), for powders made in flames with 2-L/min O_2 flow rate and BND = 5 cm. By increasing the TTIP flow rate from 1.63 g/h to 26 g/h the amount of excess oxygen in the flame is decreased and the phase composition of the product powder is changed from 85 wt. % to 18 wt. % anatase and the balance rutile (Figure 9, squares). Here, powders with more than 50 wt. % rutile made at TTIP flow rates above 16 g/h showed a bluish coloration, typical for oxygen-deficient titania (Ehrlich, 1939). This further indicates that the oxygen content of the flame plays a key role for the control of the product powder phase composition.

Investigating the anatase-rutile phase transformation during calcination in atmospheres with different oxygen partial pressure, Iida and Ozaki (1961) as well as MacKenzie (1975) reported that rutile formation can be promoted by oxygen vacancies that are created at low oxygen partial pressures. Such an influence of the combustion environment on the phase composition of titania made in a counterflow diffusion burner was also reported by Rulison et al. (1996). Anatase titania was made when feeding the $TiCl_4$ precursor in the oxidizer stream, while the introduction of the precursor in the oxygen-free fuel stream produced rutile nanoparticles. Zhu and Pratsinis (1996) reported an increase in the rutile fraction of diffusion flame-made titania nanoparticles when reducing the O_2 content of their flame by replacing oxygen with air. However, the obtained rutile weight fraction was always lower than 15 wt. %, similar to the unquenched flames here (Figure 4). The formation of up to 82 wt. % rutile (at 26 g/h TTIP flow) by use of the quenching nozzle shows that rapid quenching of the flame aerosol effectively supports the formation of rutile in flames with low oxygen content. Wu et al. (1993) reported that high quenching rates may affect the mass transport within particles and may result in the formation of metastable phases, in agreement with the formation of oxygen-deficient titania here. Hung and Katz (1992) similarly observed blue coloration in titania particles that were rapidly withdrawn from the flame by thermophoresis.

The blue coloration of the particles here was stable in air up to 300°C, at which the typical white color of titania pigment was restored (Haerudin et al., 1998). The phase composition of these powders did not change by the annealing procedure. Also, the formation of Magnéli phases Ti_nO_{2n-1}, with $n = 4$ to 10 (Andersson et al., 1957) was not observed in any of the product powder diffraction patterns, indicating that the oxygen deficiency of the titania particles was not sufficient for these phases to form or the corresponding crystal domains were too small to be detected by XRD. The stability of the suboxide in air indicates, however, that the oxygen vacancies are not only present at the particle surface, but are able to migrate into the particle center at the high particle-formation temperatures (Haerudin et al., 1998). In the laminar diffusion flame here, the oxygen partial pressure in the particle growth zone should increase with increasing distance from the burner, since more and more oxygen diffuses from the outer annular oxygen jet into the core region of the flame. This goes along with the formation of less rutile when particle growth is quenched with the nozzle at large BNDs (Figure 8).

Figure 9 shows that an increase in TTIP flow rate from 1.63 g/h to 26 g/h increases the BET−equivalent particle diameter from 15 nm to 42 nm. Since the nozzle keeps the flame length constant and the Ar, CH_4, and O_2 flow rates are constant also, the precursor/particle concentrations are the major parameters affecting particle growth here. The increase in primary-particle diameter can, thus, be attributed to faster particle growth by higher particle concentrations in the flame, in agreement with George et al. (1973) in a premixed flame, Pratsinis et al. (1996) and Jang and Kim (2001) in diffusion flames using $TiCl_4$ as the precursor. The BET data (Figure 9) indeed follow the relationship $d_p \propto V_m^{2/5}$ (thick solid line) given by Koch and Friedlander (1991) for coagulation and rapid coalescence of spherical particles in the free molecular regime, where d_p is the average particle diameter and V_m is the volume concentration of particles.

The average anatase crystallite size (Figure 9, triangles) is in good agreement with the BET−equivalent particle diameter up to 10 g/h TTIP flow rate or anatase weight fractions down to 68 wt. % (average anatase crystallite size: 30 nm; BET−equivalent particle diameter: 35 nm). When the anatase weight fraction decreases further at higher TTIP flow rates, the anatase crystallite size becomes smaller than the BET−particle diameter, indicating that particles are polycrystalline. At 26-g/h TTIP flow rate (18 wt. % anatase), where 44-nm particles are obtained, the average anatase crystallite size is only 30 nm. For the whole range of TTIP flow rates, the average rutile crystallite size (Figure 9, diamonds) is much smaller than that of anatase, but increases from 8 nm to 14 nm along with the rutile weight fraction from 15 wt. % to 82 wt. % when the TTIP flow rate is increased from 1.6 g/h to 26 g/h. There is no indication whether the product particles comprise separate anatase and rutile crystallites or whether polycrystalline pure anatase and pure rutile particles coexist next to each other, as was shown by Datye et al. (1995) for flame-made Degussa P-25.

Figure 10 is an operation diagram for the flame−nozzle process (oxygen flow rate: 2 L/min) summarizing the relationship between the BET−equivalent particle diameter with the phase composition of the product powder. Data obtained

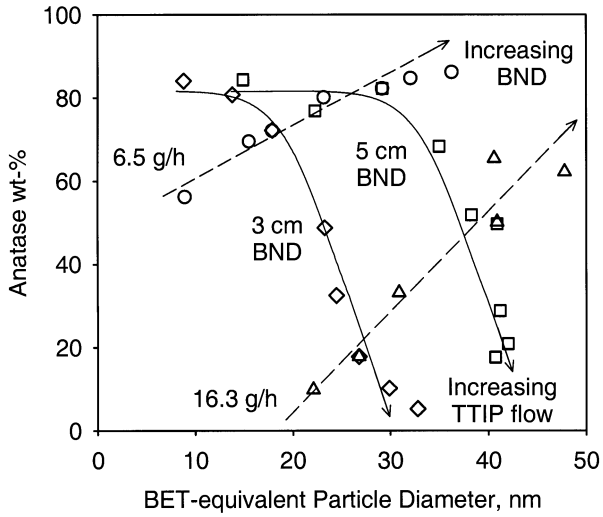

Figure 10. Operation diagram for the flame–nozzle process (2-L/min oxygen flow rate) relating BET-equivalent particle diameter and phase composition to the process parameters burner-nozzle distance (BND) and TTIP flow rate.

Powders are made at constant 6.5 g/h (circles) and 16.3 g/h (triangles) TTIP flow rate with BNDs of 1–8 cm (broken lines), and at constant 3 cm (diamonds) and 5 cm (squares) BND with 1.63–26 g/h TTIP flow rate (solid lines).

by varying the burner nozzle distance at constant 6.5 g/h (circles) and 16.3 g/h (triangles) TTIP flow rates follow the broken lines. Particles made at BND = 3 and 5 cm (Figure 9) with varying TTIP flow rates follow the solid lines. Increasing the BND from 1 cm to 8 cm at 6.5 g/h TTIP flow rate increased the BET−equivalent particle diameter from 9 nm to 36 nm and the anatase content from 56 wt. % to 85 wt. %, following the discussion of Figures 5 and 8. Increasing the BND further would finally result in the characteristics of particles made without the nozzle (60 nm, 97 wt. % anatase), since nozzle quenching becomes less effective. At 16.3-g/h TTIP flow rate, a similar increase in the BND from 2 cm to 8 cm increased the BET-equivalent particle diameter from 22 nm to 51 nm and the anatase content from 10 wt. % to 77 wt. %. The higher rutile (lower anatase) content of these powders as compared to those made with 6.5 g/h TTIP flow rate is attributed to the higher flame temperatures and lower oxygen content of the flame. At 1 cm BND and 16.3 g/h TTIP, powders with 8 nm BET-equivalent particle diameter and 28 wt. % anatase were made (not shown in Figure 10). This relatively high anatase content is attributed to higher oxygen content of the flame by increased entrainment of air at short BNDs. For each BND, the product primary particles made in flames with 16.3 g/h TTIP flow rate were larger than those made with 6.5 g/h TTIP flow rate, as higher initial particle concentrations and higher flame temperatures were employed (Figure 9).

At constant 3 and 5 cm BND, the anatase content was about 80 wt. % for TTIP flow rates of 1.63 and 3.25 g/h. Higher anatase content was only obtained at prolonged particle residence times in unquenched flames (Figure 4). A further in-

crease in TTIP flow rate to 26 g/h significantly decreased the anatase weight fraction to 5 wt. % (3 cm BND) and 18 wt. % (5 cm BND). For each TTIP flow rate, the BET−equivalent product particle size was always bigger for the larger BND, in agreement with Figure 5.

The operation diagram for the 2-L/min O_2 flame (Figure 10) shows that the size and crystallinity of flame-made titania can be effectively decoupled using the TTIP feed rate and the BND. The TTIP flow rate is more effective for control of the phase composition than the burner−nozzle distance. The BND, on the other hand, is more effective in control of the primary particle diameter. Thus, by selecting appropriate process parameters, control of the product primary-particle diameter from 8 to 51 nm and the phase composition from 85 to 5 wt. % anatase could be achieved with the nozzle. The particle-size range could be even extended to 5 nm (at 0.5-cm BND) and 60 nm (without nozzle), while the anatase content could be increased up to 97 wt. % by variation of the oxygen flow rate (Figure 4).

Conclusions

A flame aerosol process for precise control of product particle size, morphology, and phase composition was developed and performance-tested for synthesis of titania nanoparticles. The process relies on rapid quenching of the flame aerosol with a critical flow nozzle placed at the desired positions in front of the particle-laden flame. While the upstream flame temperatures are not significantly influenced by the nozzle, high-temperature gradients across the nozzle are achieved by flow expansion and mixing with entrained ambient air. This quenching procedure rapidly slows down particle growth downstream of the nozzle, thus "freezing" the particle size and morphology of the upstream aerosol. The BET−average primary particle size could be precisely controlled from 5 nm to 60 nm by selecting the burner−nozzle distance.

Virtually nonagglomerated and spherical titania particles were made. An operation diagram showed that the phase composition of the product powder could be independently controlled from 85 wt. % to 5 wt. % anatase and the balance rutile by introducing and stabilizing oxygen vacancies in the titania particles with the quenching procedure. This broad operation window with respect to product particle size, morphology, and crystallinity shows the high potential of the flame−nozzle process for a successful application to other flame configurations and the cost-effective synthesis of silica, alumina, and other oxide and nonoxide ceramics, and even carbon black and metals like nickel and iron with controlled size, crystallinity, and a limited degree of agglomeration. The formation of substoichiometric (blue) titania by nozzle quenching shows that the flame−nozzle process can even produce novel metastable materials.

Acknowledgment

This work was supported by ETH-Gesuch 33/99-2 and the Swiss Commission for Technology and Innovation (CTI), TopNano21 Grant 5978.2 TNS, and was presented at the AIChE 2002 Annual Meeting (Session 389b). We thank Dr. Frank Krumeich (ETH) for the HRTEM investigations.

Literature Cited

Andersson, S., B. Collén, U. Kuylenstierna, and A. Magnéli, "Phase Analysis on the Titanium-Oxygen System," *Acta Chem. Scand.*, **11**, 1641 (1957).

Arabi-Katbi, O. I., S. E. Pratsinis, P. W. Morrison, Jr., and C. M. Megaridis, "Monitoring the Flame Synthesis of TiO_2 Particles by in-situ FTIR Spectroscopy and Thermophoretic Sampling," *Combust. Flame*, **124**, 560 (2001).

Barringer, E., N. Jubb, R. Fegley, R. L. Pober, and H. K. Bowen, "Processing of Monosized Powders", *Ultrastructure Processing of Ceramics, Glasses, and Composites*, L. L. Hench and D. R. Ulrich, eds., Wiley, New York, p. 315 (1984).

Bradley, D. C., R. C. Mehrotra, and D. P. Gaur, *Metal Alkoxides*, Academic Press, London, p. 56 (1978).

Calcote, H. F., W. Felder, D. G. Keil, and D. B. Olson, "A New Flame Process for Synthesis of Si_3N_4 Powders for Advanced Ceramics," *Proc. Combust. Inst.*, **23**, 1739 (1990).

Calcote, H. F., and W. Felder, "A New Gas-Phase Combustion Synthesis Process for Pure Metals, Alloys, and Ceramics," *Proc. Combust. Inst.*, **24**, 1869 (1992).

Cheary, R. W., and A. J. Coelho, "A Fundamental Parameter Approach to X-Ray Line-Profile Fitting," *Appl. Crystallogr.*, **25**, 109 (1992).

Datye, A. K., G. Riegel, J. R. Bolton, M. Huang, and M. R. Prairie, "Microstructural Characterization of a Fumed Titanium Dioxide Photocatalyst," *J. Solid State Chem.*, **115**, 236 (1995).

Dobbins, R. A., and C. M. Megaridis, "Morphology of Flame-Generated Soot as Determined by Thermophoretic Sampling," *Langmuir*, **3**, 254 (1987).

Dufaux, D. P., and R. L. Axelbaum, "Nanoscale Unagglomerated Nonoxide Particles from a Sodium Coflow Flame," *Combust. Flame*, **100**, 350 (1995).

Ehrlich, P., "Phasenverhältnisse und magnetisches Verhalten im System Titan/Sauerstoff," *Z. Elektrochem.*, **45**, 362 (1939).

Formenti, M., F. Juillet, P. Meriaudeau, S. J. Teichner, and P. Vergnon, "Preparation in a Hydrogen-Oxygen Flame of Ultrafine Metal Oxide Particles," *J. Colloid Interface Sci.*, **39**, 79 (1972).

George, A. P., R. D. Murley, and E. R. Place, "Formation of TiO_2 Aerosol from the Combustion Supported Reaction of $TiCl_4$ and O_2," *Symp. Faraday. Soc.*, **7**, 63 (1973).

Glassman, I., K. A. Davis, and K. Brezinsky, "A Gas-Phase Combustion Synthesis Process for Non-Oxide Ceramics," *Proc. Combust. Inst.*, **24**, 1877 (1992).

Glumac, N. G., Y. J. Chen, G. Skandan, and B. Kear, "Scalable High-Rate Production of Non-Agglomerated Nanopowders in Low Pressure Flames," *Mater. Lett.*, **34**, 148 (1998).

Haerudin, H., S. Bertel, and R. Kramer, "Surface Stoichiometry of 'Titanium Suboxide.' Part I: Volumetric and FTIR Study," *J. Chem Soc. Faraday Trans.*, **94**, 1481 (1998).

Hansen, J. P., J. R. Jensen, H. Livbjerg, and T. Johannessen, "Synthesis of ZnO Particles in a Quench-Cooled Flame Reactor," *AIChE J.*, **47**, 2413 (2001).

Hung, C. H., and J. L. Katz, "Formation of Mixed Oxide Powders in Flames. Part I: TiO_2-SiO_2," *J. Mater. Res.*, **7**, 1861 (1992).

Iida, Y., and S. Ozaki, "Grain Growth and Phase Transformation of Titanium Oxide During Calcination," *J. Amer. Ceram. Soc.*, **44**, 120 (1961).

Jang, H. D., and S. K. Kim, "Controlled Synthesis of Titanium Dioxide Nanoparticles in a Modified Diffusion Flame Reactor," *Mater. Res. Bull.*, **36**, 627 (2001).

Johannessen, T., S. E. Pratsinis, and H. Livbjerg, "Computational Analysis of Coagulation and Coalescence in the Flame Synthesis of Titania Particles," *Powder Technol.*, **118**, 242 (2001).

Koch, W., and S. K. Friedlander, "Particle Growth by Coalescence and Agglomeration," *Part. Part. Syst. Charact.*, **8**, 86 (1991).

Lindackers, D., M. G. D. Strecker, P. Roth, C. Janzen, and S. E. Pratsinis, "Formation and Growth of SiO_2 Particles in Low Pressure H_2/O_2/Ar Flames Doped with SiH_4," *Combust. Sci. Technol.*, **123**, 287 (1997).

MacKenzie, K. J. D., "The Calcination of Titania. VI. The Effect of Reaction Atmosphere and Electric Fields on the Anatase-Rutile Transformation," *Trans. J. Brit. Ceram. Soc.*, **74**, 121 (1975).

Perry, R. H., and D. Green, *Perry's Chemical Engineering Handbook*, 6th ed., McGraw-Hill, New York, p. 5 (1984).

Pratsinis, S. E., W. Zhu, and S. Vemury, "The Role of Gas Mixing in Flame Synthesis of Titania Powders," *Powder Technol.*, **86**, 87 (1996).
Pratsinis, S. E., "Flame Aerosol Synthesis of Ceramic Powders," *Prog. Energy Combust. Sci.*, **24**, 197 (1998).
Rulison, A. J., P. F. Miquel, and J. L. Katz, "Titania and Silica Powders Produced in a Counterflow Diffusion Flame," *J. Mater. Res.*, **11**, 3083 (1996).
Stark, W. J., K. Wegner, S. E. Pratsinis, and A. Baiker, "Flame Aerosol Synthesis of Vanadia-Titania Nanoparticles: Structural and Catalytic Properties in the Selective Catalytic Reduction of NO by NH_3," *J. Catal.*, **197**, 182 (2001).
Ulrich, G. D., B. A. Milnes, and N. S. Subramanian, "Particle Growth in Flames. II: Experimental Results for Silica Particles," *Combust. Sci. Technol.*, **14**, 243 (1976).
Ulrich, G. D., "Flame Synthesis of Fine Particles," *Chem. Eng. News*, **62**, 22 (1984).
Wegner, K., and S. E. Pratsinis, "Aerosol-Based Flame Synthesis: A Microreactor for Silica Nanoparticles," *Innovative Processing of Films and Nanocrystalline Powders*, Vol. 18, K. L. Choy, ed., Imperial College Press, London, p. 193 (2002).
Wegner, K., W. J. Stark, and S. E. Pratsinis, "Flame-Nozzle Synthesis of Nanoparticles with Closely Controlled Size, Morphology and Crystallinity," *Mater. Lett.*, **55**, 318 (2002).
Wu, M. K., R. S. Windeler, C. K. R. Steiner, T. Börs, and S. K. Friedlander, "Controlled Synthesis of Nanosized Particles by Aerosol Processes," *Aerosol Sci. Technol.*, **19**, 527 (1993).
Zhu, W., and S. E. Pratsinis, "Flame Synthesis of Nanosize Particles: Effect of Flame Configuration and Oxidant Composition," *Nanotechnology*, G. M. Chow, K. E. Gonsalves, eds., ACS Symp. Ser., Vol. 622, ACS, Washington, DC, p. 64 (1996).

Manuscript received July 12, 2002, and revision received Jan. 3, 2003.